analytical chemistry

pubs.acs.org/ac
Article

Comprehensive Impurity Profiling of mRNA: Evaluating Current Technologies and Advanced Analytical Techniques

Julien Camperi,* Steffen Lippold, Luladey Ayalew, Brian Roper, Stephanie Shao, Emily Freund, Ariane Nissenbaum, Carolina Galan, Qinjingwen Cao, Feng Yang, Christopher Yu, and Axel Guilbaud*

Cite This: Anal. Chem. 2024, 96, 3886−3897

ABSTRACT: In vitro transcription (IVT) of mRNA is a versatile platform for a broad range of biotechnological applications. Its rapid, scalable, and cost-effective production makes it a compelling choice for the development of mRNA-based cancer therapies and vaccines against infectious diseases. The impurities generated during mRNA production can potentially impact the safety and efficacy of mRNA therapeutics, but their structural complexity has not been investigated in detail yet. This study pioneers a comprehensive profiling of IVT mRNA impurities, integrating current technologies with innovative analytical tools. We have developed highly reproducible, efficient, and stability-indicating ion-pair reversed-phase liquid chromatography and capillary gel electrophoresis methods to determine the purity of mRNA from different suppliers. Furthermore, we introduced the applicability of microcapillary electrophoresis for high-throughput (<1.5 min analysis time per sample) mRNA impurity profiling. Our findings revealed that impurities are mainly attributed to mRNA variants with different poly(A) tail lengths due to aborted additions or partial hydrolysis and the presence of double-stranded mRNA (dsRNA) byproducts, particularly the dsRNA 3′-loop back form. We also implemented mass photometry and native mass spectrometry for the characterization of mRNA and its related product impurities. Mass photometry enabled the determination of the number of nucleotides of different mRNAs with high accuracy as well as the detection of their size variants [i.e., aggregates and partial and/or total absence of the poly(A) tail], thus providing valuable information on mRNA identity and integrity. In addition, native mass spectrometry provided insights into mRNA intact mass, heterogeneity, and important sequence features such as poly(A) tail length and distribution. This study highlights the existing bottlenecks and opportunities for improvement in the analytical characterization of IVT mRNA, thus contributing to the refinement and streamlining of mRNA production, paving the way for continued advancements in biotechnological applications.

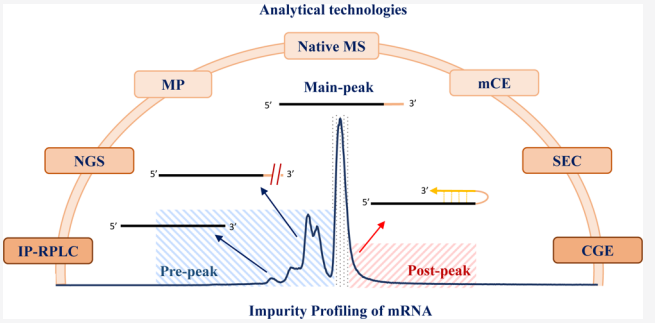

INTRODUCTION

The introduction of synthetic mRNA (known as in vitro-transcribed mRNA) into the field of molecular biology has been a revolutionary development with far-reaching implications. It serves as a versatile tool for the rapid, transient expression of peptides and proteins in the cytoplasm of host cells. This innovation is highlighted by its usefulness in a range of applications, from potential replacement of defective proteins to antigen presentation for vaccine development.[1,2] Since the early 2000s, the influence of in vitro transcription (IVT) mRNA in the field of medical therapeutics has become even more profound when considering its pivotal role in cancer immunotherapy, where numerous drug candidates have advanced into clinical trials.[3,4] Meanwhile, advanced technologies in genome engineering use IVT mRNA-encoded designer nucleases, in vivo delivery of IVT mRNA, and IVT mRNA-based pluripotent stem cell generation.[5] These new pathways highlight the versatility and adaptability of IVT mRNA as a powerful tool in modern molecular and cellular biology. In a comparative context, IVT mRNA stands out for several inherent advantages over traditional DNA- or protein-based therapeutic modalities as drug candidates.[6] In particular, IVT mRNA does not integrate into the host genome, reducing the risk of insertional mutagenesis—a key concern in gene therapy and genetic medicine.[7] Compared to other protein-based biologics, the design of IVT mRNA is also more straightforward, which allows for rapid, scalable, and cost-effective production, an important feature in scenarios where rapid vaccine development and large-scale production are paramount, as exemplified during the COVID-19 pandemic.

Received: December 5, 2023
Revised: January 24, 2024
Accepted: February 12, 2024
Published: February 20, 2024

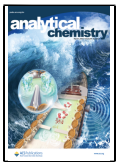

The unique properties of IVT mRNA molecules add complexity to their characterization. These polar molecules exert a strong negative charge and contain secondary structures and important sequence features including 5′Cap, 5′- and 3′-untranslated regions (UTRs), open reading frame (ORF), and poly(A) tail. The structural integrity of these elements has a direct impact on the mRNA efficiency. Any disruption, whether due to hydrolysis, RNases, or aborted transcription, can lead to the formation of fragmented mRNA molecules unable to translate a complete ORF and, consequently, unable to perform their intended function. Despite the recent success of mRNA-based therapies and vaccine development and approval, the analytical characterization of IVT mRNA remains a major challenge.

Several analytical methods are commonly used for mRNA characterization and are employed in quality control (QC) environments to support batch release and stability and assess critical quality attributes (CQAs) at different stages of the drug life cycle, including production and storage.[8,9] Purity is usually assessed by ion-pair reversed-phase liquid chromatography (IP-RPLC) by measuring product-related impurities, such as short mRNA fragments,[10−14] while integrity is usually confirmed by determining mRNA length by capillary gel electrophoresis (CGE).[15,16] As an alternative, Raffaele et al. demonstrated the value of using on-chip capillary electrophoresis to determine the purity and integrity of 2000-nucleotide (nt) mRNA in lipid nanoparticle vaccines.[17] Recently, considerable efforts have been made to improve the separation, sensitivity, applicability, and turnaround times of the HPLC-based methods. For example, the choice of the IP-RPLC column, the composition of the mobile phase using an ion-pairing agent, and the column temperature have been studied for short 100-nt RNAs.[10,18] Regarding the analysis of long mRNAs, Kuwayama et al. reported the interest in using an octadecyl-based RPLC column with superwide pores for achieving higher separation.[19] Similarly, an ultrawide pore size exclusion chromatography (SEC) column has been recently introduced for efficient separation of mRNA aggregates and lipid nanoparticles.[20] Additionally, mass photometry (MP) was recently introduced as an interferometric mass spectrometry (MS) methodology capable of measuring the mass and relative abundance of biomolecules in solutions.[21] However, further studies are needed to understand the extent to which MP's capabilities apply to nucleic acids[22] and in particular to mRNA characterization. It should also be noted that MS-based methods have also been widely developed for characterizing mRNA critical structural features, such as poly(A) tail length and distribution[23,24] and 5′ end-capping efficiency,[25] but few studies have reported the use of MS for intact mass analysis of large mRNAs (i.e., >200 nts).[26,27] Brophy et al. reported the analysis of EPO mRNA (858 nts), Fluc mRNA (1909 nts), and Cas9 mRNA (4521 nts) using IP-RPLC—time of flight MS and charge detection MS methods.[27] While some signals have been extracted from their analysis, the resulting MS profiles were not satisfactory enough to get an accurate determination of molecular weights (MWs). Although advances in analytical methods have been made for characterizing mRNA (in particular for short RNA molecules, i.e., ≤100 nts), further improvements are still required to achieve a better understanding of larger mRNAs and their related impurities.

In this study, we performed comprehensive impurity profiling of different mRNAs by combining the current analytical methods and novel technologies. This analytical toolbox provided crucial insights into the nature of all mRNA variants, including mRNAs with different poly(A) tail lengths due to aborted additions or partial hydrolysis, and the presence of covalent and noncovalent aggregates that may be associated with different types of double-stranded mRNA (dsRNA) byproducts occurring during the IVT process. While purity profiles of different mRNAs (in terms of length and structures) were obtained using optimized IP-RPLC and CGE methods as well as microcapillary electrophoresis (mCE) and SEC, the nature of the impurities has been further investigated using direct RNA sequencing NGS, MP, and native MS technologies. Holistically, these methods have provided valuable information about the profile of mRNA impurities and an understanding of their potential impact on mRNA-based applications.

MATERIALS AND METHODS

mRNA Samples. The eGFP mRNA (996 nts) sample was purchased from GenScript (Piscataway, NJ), TriLink BioTechnologies (San Diego, California, CA), and Oz Biosciences (San Diego, CA); Fluc mRNA (1909 nts) from GenScript (Piscataway, NJ) and Oz Biosciences (San Diego, CA); and beta gal mRNA (3420 nts) from TriLink BioTechnologies (San Diego, California, CA). The vendors will be named "A, B, and C". The samples were available at 1 mg/mL in the formulation buffer (10 mM sodium citrate, pH 6.4) and kept at −80 °C until use. The mRNAs were modified with 5-methoxyuridine (5 moU) residues, 3′-poly(A) tail (100−120 nts), and 5′-CleanCap1 (TriLink BioTechnologies). In addition, in-house IVT mRNAs using the same features were also produced using the protocol provided in Experimental Section S1. Samples subjected to heat-stress conditions were incubated at 37 °C for 5 days in the formulation buffer at 1 mg/mL. These stress conditions were based on an internal procedure.

IP-RPLC−UV Analysis. Measurements were carried out on an ACQUITY UPLC H-Class system (Waters, Milford, MA) equipped with a quaternary solvent delivery pump, autosampler, and UV detector. The HPLC system was controlled by Chromeleon software (revision edition C.01.07 SR4 [505]) from Thermo Fisher Scientific (Santa Clara, CA). RNA samples were separated using a DNAPac RP column (2.1 mm I.D. × 100 mm, 4.0 μm) from Thermo Fisher (Sunnyvale, CA). Buffer A was an aqueous solution of 50 mM TEA and 50 mM HFIP in water at pH 9.3, and buffer B was an organic solution of 25 mM TEA and 25 mM HFIP in 90% (v/v) methanol. IP-RPLC analyses were performed using the following gradient conditions: flow rate of 0.4 mL/min, 5% B over 1.0 min to 18% B over 19 min, to 70% B over 1 min, before decreasing and holding at 5% B for 5 min. The column temperature was 80 °C. The UV detector was set at 260 nm.

CGE−Laser-Induced Fluorescence Analysis. CGE experiments were performed on a PA800 plus instrument equipped with a 488 nm excitation laser (520 nm bandpass filter), laser-induced fluorescence (LIF) detection, and 32Karat v9.0 acquisition software (AB Sciex, Framingham, MA). RNA analysis was performed using the SCIEX RNA 9000 Purity and Integrity kit from Sciex with the SYBR Green II RNA Gel Stain. Electrophoretic separations occurred in a 50 μm-internal diameter (ID) uncoated fused-silica capillary at 12 kV constant voltage for 100 min (reverse polarity) with a capillary length of 60 cm. The capillary temperature was 15 °C. Samples were pressure-injected at 2 psi for 10 s with a 2 psi 10 s water plug

https://doi.org/10.1021/acs.analchem.3c05539
Anal. Chem. 2024, 96, 3886−3897

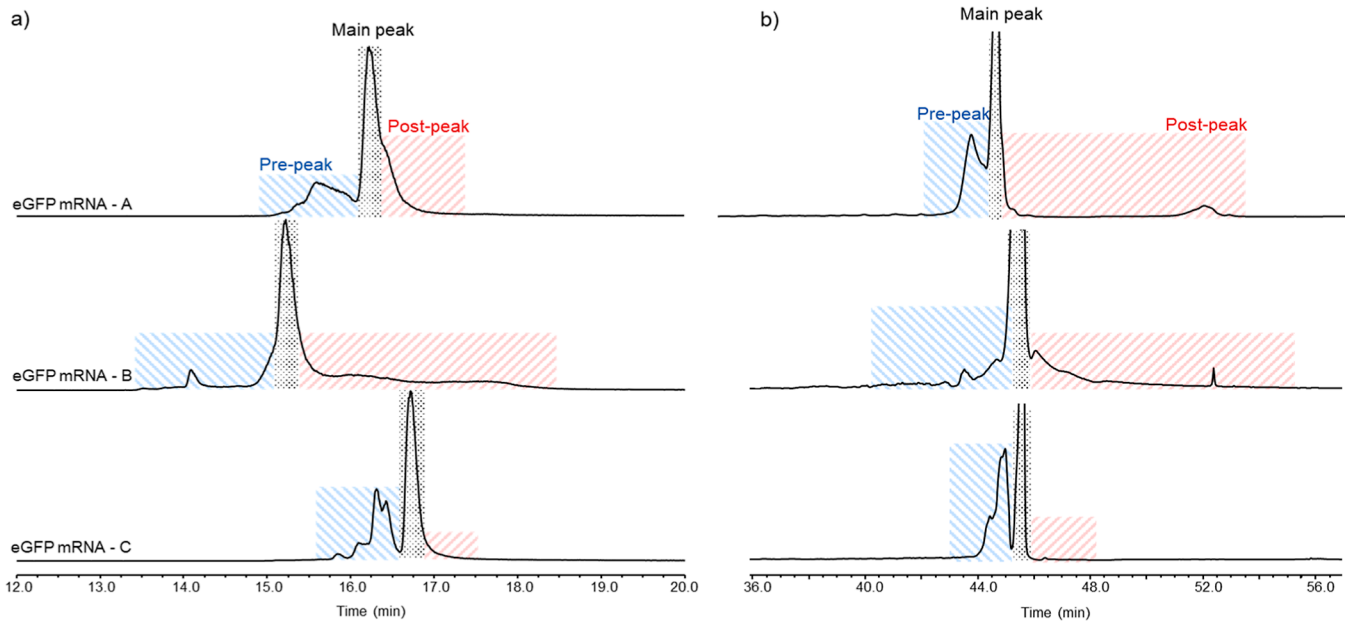

Figure 1. Analysis of three eGFP mRNAs obtained from different suppliers (A, B, and C) by IP-RPLC−UV (a) and CGE−LIF (b) methods for purity assessment. Prepeak, main peak, and postpeak regions are highlighted by blue, black, and red boxes, respectively. The difference in retention and migration time of the main peak between batches of eGFP mRNA is due to the different compositions and lengths of the 5′- and 3′- UTR sequences between suppliers.

pressure injected prior to the sample. Raw data was transferred from an integrated analysis software (32Karat) to Chromeleon (edition revision C.01.07 SR4 [505]) software for data analysis.

mCE−LIF Analysis. mCE experiments were performed on a LabChip GXII using RNA LabChips (catalog no. 760435) and RNA assay reagent kits (catalog no. CLS960010) from PerkinElmer (Waltham, MA). Samples were diluted in water to 100 ng/μL before transferring 3 μL of diluted mRNA to a 96-well PCR plate and were then heated at 70 °C for 10 min and subsequently cooled on ice for 5 min or kept on ice. Samples were then diluted using a 1× sample buffer from the RNA reagent kit to a final sample volume of 50 μL (6.25 ng/μL). The RNA LabChip was prepared according to the manufacturer's manual.

In the LabChip, a gel-sieving matrix containing a blue fluorescent dye was injected into the separation channel, and then the sample was electrokinetically injected and mRNA binds to the dye. Voltage is applied, and mRNA mobilizes and separates through the sieving gel matrix according to size. The mRNA signal is observed by laser-induced fluorescent detection. The separation time is 70 s for each sample to cover the range of 50−6000 nts of RNA size. The electropherogram for each injection was transferred to Chromeleon (edition revision C.01.07 SR4 [505]) software from Thermo Fisher Scientific (Santa Clara, CA) for data analysis. For each sample, prepeak, main peak, and post-peak impurities are calculated as a percentage of the total corrected peak area, and the mRNA purity or integrity is reported as the percent corrected peak area of the main peak.

SEC−UV Analysis. The mRNA samples were separated using an SRT(R) SEC-1000 gel filtration column (4.6 mm I.D. × 300 mm, 5 μm particle size, 1000 Å, stainless steel) purchased from Sepax Technologies, Inc. (Newark, DE), and a mobile phase composed of 100 mM Tris−HCl and 300 mM NaCl at pH 7.5. The injection volume was 10 μL, and the separation was operated at 25 °C with a flow rate of 0.350 mL/min. A diode array detector was used for recording the UV signal at 260 nm.

MP Analysis. MP measurements were carried out on a TwoMP Auto instrument (Refeyn, UK) at room temperature, i.e., approximately 24 °C. High-precision microscope cover glasses, 24 mm × 50 mm, Thorlabs CG15KH were used and coated with poly-L-lysine (PLL). PLL is positively charged and is used to increase the amount of binding events of negatively charged nucleic acids, which greatly increases detection. Samples were diluted in a PBS buffer and a final mRNA amount of 50 ng in droplets was analyzed. For each experiment, thousands of mRNA molecules were counted and their contrasts were measured. Standardized ssRNA ladder (New England Biolabs, cat# N0364) calibration was used to determine the number of nucleotides. Movie acquisition was performed for 60 s with the DiscoverMP software (version 2022 R1, Refeyn Ltd.), and the data were analyzed using the range tool parameters for more accurate mass and purities. Data was analyzed using DiscoverMP v2.0.

Intact mRNA Analysis by MS. Prior to intact mass analysis, samples were buffer-exchanged to 200 mM ammonium acetate using a molecular 10 to 50 kDa cutoff filter (Millipore Sigma, MA). A minimum of 20 μg was diluted with 200 mM ammonium acetate to a total volume of 500 μL. Five repeats of buffer exchange were performed using 10,000 g for 5 min, and the samples were concentrated in the final step to a volume of 20 to 100 μL resulting in a final concentration in a range from 0.2 to 1 μg/μL. 15 microliters of buffer-exchanged samples were loaded into a borosilicate emitter (Thermo Fisher Scientific). The analysis was performed on an Orbitrap Q Exactive UHMR mass spectrometer equipped with a Nanospray Flex ion source (Thermo Fisher Scientific, Santa Clara, CA). Data were acquired in an m/z range of 350 to 15,000. Electrospray ionization was performed in positive mode using a spray voltage of 1.4 kV. Source parameters

https://doi.org/10.1021/acs.analchem.3c05539
Anal. Chem. 2024, 96, 3886−3897

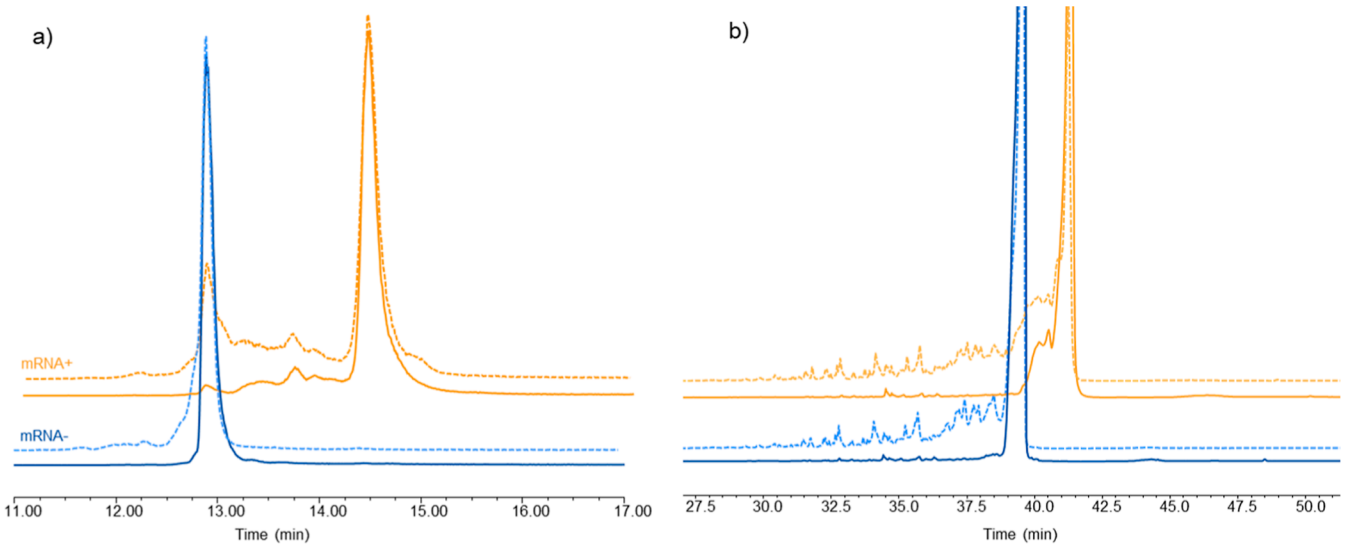

Figure 2. Comparison of purity profiles between two short mRNAs that differ only in the absence or presence of a 100 nt poly(A) tail (mRNA+ and mRNA−). (a) IP-RPLC and (b) CGE profiles were obtained for mRNA− (bottom traces) and mRNA+ (top traces). Separation profiles were obtained for samples exposed to an elevated temperature of 37 °C for 5 days (striped traces) versus control (solid traces).

(desolvation voltages and ion transfer tube temperature) and mass analyzer conditions (resolution and trapping gas) were optimized to resolve mRNA heterogeneity. The ion transfer capillary temperature was kept at 250 °C. An in-source collision-induced dissociation energy of 25/30 eV and −50/−125 V in-source trapping desolvation voltages were used for poly(A) tail and intact mRNA analysis, respectively. The S-lens RF level was set at 200. Nitrogen was applied as the collision gas, and the trapping gas was set to 5 (ultrahigh vacuum around $2.6 \times 10 \times 10^{-10}$). The resolution was set to 200,000 [poly(A) tail sample] or 6000 (intact mRNA). All data were visually inspected in FreeStyle (v 1.8) and deconvoluted using FreeStyle for isotopically resolved poly(A) tail or UniDec (v 6.0.3.) for intact mRNA data.

RESULTS AND DISCUSSION

Development of LC and CE Methods for mRNA Purity Assessment. *IP-RPLC and CGE Methods.* Consistent manufacturing of high-quality IVT mRNA is critical to the overall success of any mRNA-based therapeutic product. Both IP-RPLC and CGE techniques are commonly used for mRNA characterization. Purity assessment by IP-RPLC typically involves high column temperature and the use of an ion-pairing agent in combination with an organic solvent, while integrity determination by CGE involves the use of high quantities of a denaturing agent (e.g., formamide or 4−8 M urea under nonaqueous conditions).[8] In both methods, denaturing conditions improve the mRNA separation by disrupting base-pairing and base-stacking interactions. mRNA is thus linearized, enabling sharper peaks to be separated and eluted.

A typical purity profile of eGFP mRNA (~996 nts) shows three regions (pre-peak, main peak, and post-peak) and differs drastically between suppliers (Figure 1). To achieve a high separation of mRNA variants in IP-RPLC, a DNAPac RP column with a 4 μm large-pore spherical polymer resin, with a mobile phase containing TEA/HFIP in methanol at pH 9.3, was used (see Figure 1a). For CGE, different parameters were optimized to improve injection repeatability and resolution. First, peak repeatability was optimized with pressure injections, which ranged from 5 to 10% relative standard deviation (RSD) for the different analyzed samples, compared with 16 to 26% RSD with electrokinetic injections. Second, a lower capillary temperature was preferred (15 °C vs 30 °C) to improve postpeak separation (Figure S1). Electropherograms obtained by using the optimized conditions are shown in Figure 1b. It should be noted that the analysis time for the CGE method is almost 2.5 times longer than for the IP-RPLC method. The repeatability of IP-RPLC and CGE separations were also assessed by performing triplicate analyses. The results showed good repeatability in terms of % purity (main peak) for both methods, with RSD values below 1.8 and 0.7% for IP-RPLC and CGE, respectively (see Table S1).

The different eGFP mRNA purity profiles observed between suppliers highlight the impact of the manufacturing process (upstream and downstream) on mRNA quality. Higher purities were measured for eGFP mRNA B, with values of ~63 and ~64% obtained by IP-RPLC and CGE, respectively. Several variants migrating to the left of the intact mRNA peak, corresponding to smaller mRNA fragments, were observed for all samples, with a higher level for eGFP mRNA C. Both methods also indicated that eGFP B has the highest level of postpeaks, which may be associated with high MW (HMW) species. The percentages of prepeaks, main peaks, and postpeaks are summarized in Table S1.

Overall, similar levels of impurities in the prepeak and postpeak regions were measured between the two methods. However, the levels of postpeak impurities are slightly lower with CGE, mainly due to a better separation of these variants compared to IP-RPLC. For example, for eGFP A mRNA, while the postpeak coelutes with the main peak in IP-RPLC, we observe a baseline separation in CGE, with a time difference of around 8 min between the main peak and the postpeak. The improved resolution in CGE was attributed to a decreased level of mRNA secondary structures due to stronger denaturing conditions. We also demonstrated the broad applicability of IP-RPLC and CGE for larger mRNAs up to 4500 nts, showing a negative correlation between resolution and number of nucleotides (see Figure S2). Both IP-RPLC and

https://doi.org/10.1021/acs.analchem.3c05539
Anal. Chem. 2024, 96, 3886−3897

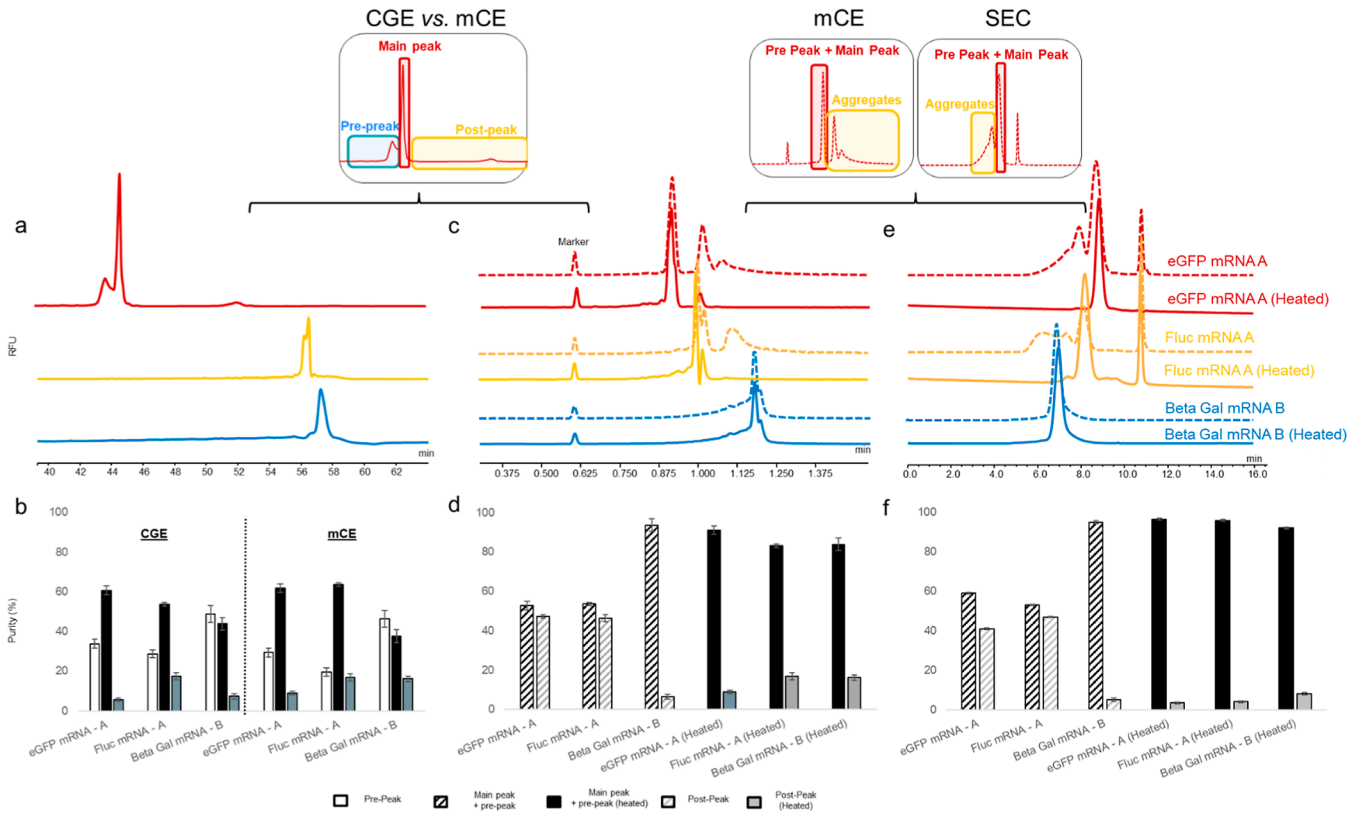

Figure 3. Comparative analysis of mRNA purity using (a) CGE, (c) mCE, and (e) SEC. Three different mRNAs (eGFP, Fluc, and beta gal mRNA) from vendors A and B were analyzed under denaturing (70 °C for 10 min, solid lines) and native (dashed lines) conditions. (b) For comparability of CGE and mCE under denaturing conditions, percentages of prepeak (white bars), main peak (black bars), and postpeak (gray bars) were reported. (d,f) For mCE and SEC comparability, pre- and main peaks were integrated together and compared to the postpeak region corresponding to aggregates. Compared with mCE, SEC profiles are inverted, with aggregates appearing on the left and monomers/short impurities on the right. For each mRNA, the percentages of prepeak/main peak (black striped or solid bars for native and denaturing conditions, respectively) and postpeak (gray striped or solid bars for native and denaturing conditions, respectively) were calculated. Each sample was injected three times and bars represent the mean ± SD.

CGE methods can be used to assess the purity of large mRNAs of the relevant sizes.

Impact of a Poly(A) Tail on IP-RPLC and CGE Profiles. The length and distribution of the poly(A) tail impact the separation profiles. As shown in Figure 1, the main peak obtained for eGFP B mRNA is slightly wider than that for the other samples. Poly(A) tail analysis (see Experimental Section S2) revealed that the tail length of eGFP B mRNA is around 120 nts, compared with 100 nts for the other mRNA samples (see Figure S3), but also showed the presence of an even longer poly(A) tail population, contributing to increased heterogeneity separation profiles. This difference in length also explains why eGFP B migrates more slowly in CGE than other mRNAs.

To better understand the impact of the poly(A) tail, we then synthesized two short in-house IVT mRNAs, with identical ORFs and structural features, except for the absence or presence of a 100 nt poly(A) tail, denoted by mRNA− (683 nts) and mRNA+ (783 nts). Interestingly, we noticed that the main peak of the mRNA− sample has a similar retention time (i.e., 12.8 min) to the first prepeak present in the mRNA+ sample, suggesting that the poly(A) tail-less variant is an impurity present in the prepeak region (Figure 2a). Also, the chromatogram obtained from mRNA+ reveals the presence of several prepeaks between the poly(A) tail-less peak and the main peak, whose identities have yet to be determined (Figure 2a, top solid trace). In CGE, the electropherograms show a shift in migration time of 3 min of the main peak when the poly(A) tail is present (see Figure 2b), demonstrating that CGE separates according to the length of the mRNA molecules. We also notice the presence of a shoulder before the main peak of mRNA+ (Figure 2b, top traces), which is attributed to the presence of a poly(A) tail. This shoulder is not observed for eGFP mRNA (Figure 1b) due to its larger size and, thus, lower resolution power of the CGE separation.

The two mRNA samples were then subjected to heat stress to see any potential degradation or change in purity (Figure 2a,b, striped lines). Both IP-RPLC and CGE methods indicated that the poly(A) tail is mainly degraded during heat stress. First, the tail-less peak increases by ∼24% in IP-RPLC compared to the control sample, while slight increases in impurities were observed in prepeak and postpeak regions. Interestingly, CGE offers a better separation of prepeaks for the stressed samples (see Figure 2b). An increase of ∼30% was measured for both mRNA+ and mRNA− samples compared with the control samples. These impurities can be associated with small RNA fragments resulting from hydrolysis and/or modifications such as depyrimidination, etc. and can be potentially confirmed by oligonucleotide mapping via MS.[28] In addition, the previously observed shoulder in mRNA+ is also impacted with an increase of 14%. The percentages of

https://doi.org/10.1021/acs.analchem.3c05539
Anal. Chem. 2024, 96, 3886−3897

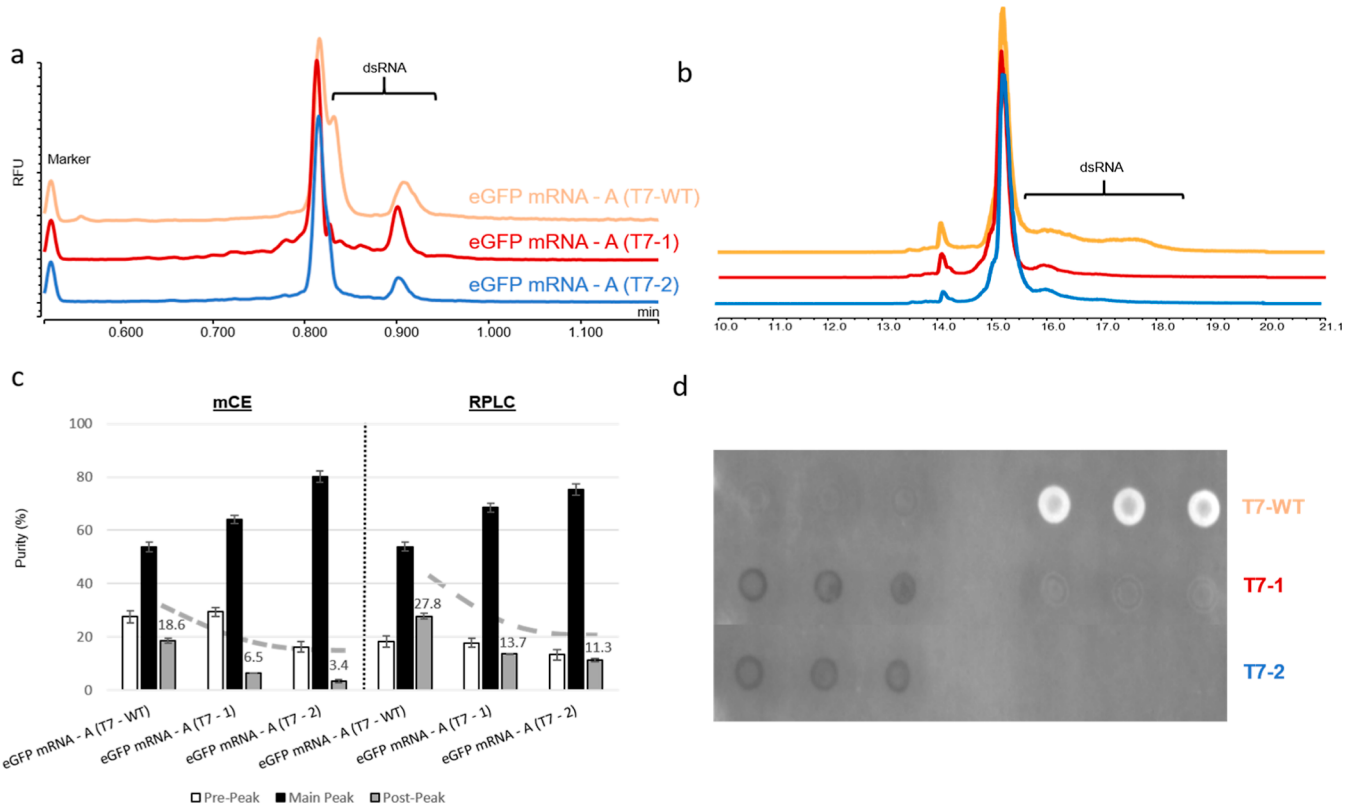

Figure 4. Impact of T7 polymerase on the dsRNA 3′-loop back byproducts' formation during IVT reaction. mCE (a) and IP-RPLC (b) methods were used independently to assess the dsRNA levels of in-house eGFP mRNA constructs synthesized using three different T7 polymerases (T7-WT in orange, T7-1 in red, and T7-2 in blue) under denaturing conditions. (c) For each condition, the percentage of prepeak (white), main peak (black), and postpeak (corresponding to dsRNA in gray) was reported (refer to Figure 3 for the definition of pre- and postpeak regions). The gray striped line represents the trend of dsRNA levels under the different conditions. Each sample was injected three times and bars represent the mean ± SD. (d) Dot blot for different conditions (see Experimental Section S3); mRNAs were stained using an anti-dsRNA mIgG2a monoclonal antibody. Each sample was stained three times individually, as represented by the three dots.

prepeaks, main peaks, and postpeaks are summarized in Table S2.

The profiles clearly show that the addition of the poly(A) tail increases the level of impurities in the prepeak region. Further investigations have shown that a high level of prepeak is usually obtained when a longer tail is added (see Figure S4).

Under stress conditions, prepeak impurities are mainly impacted, due to the loss of the poly(A) tail, while no changes are observed in postpeak regions. These observations are in agreement with the literature.[29] Loss of the poly(A) tail has a negative impact on mRNA functionality, leading to a defective product, underlining the importance of monitoring prepeak regions during stability studies.

Overall, the data show that the IP-RPLC and CGE methods are highly comparable and we have succeeded in demonstrating the presence of a poly(A) tail-less mRNA variant in the prepeak region, as well as the impact of a poly(A) tail on the separation profiles.

mCE for the Determination of Purity and Aggregate Content of mRNA. We demonstrated that CGE is an excellent technique for achieving high mRNA separation efficiency, with better resolution for postpeak impurities due to its stronger denaturation conditions than those of the IP-RPLC method. However, separation times are relatively long (between 40 and 60 min), which currently limits this approach to widespread mRNA analysis. Recently, two studies have reported the separation potential of microcapillary electrophoresis for oligonucleotides[26] and mRNA in lipid nanoparticle vaccines,[17] offering short turnaround time, acceptable resolution, and the potential to increase sample throughput.

To evaluate this analytical tool, a comprehensive comparison between conventional CGE and mCE (focusing on the purity assessment of several mRNAs under denaturing conditions) was carried out, with particular emphasis on prepeak, main peak, and postpeak mRNA percentages (see Figure 3a–d). The data confirm similar trends in terms of purity between the methods, with close values obtained for the levels of prepeak, main peak, and postpeak (see Figure 3b). This congruence highlights the reliability and reproducibility of results obtained through mCE, in terms of separation efficiency, compared to the traditional CGE. This comparative analysis suggests that mCE represents a promising advancement in mRNA purity assessment, offering similar separation efficiency, data quality, and shorter run times (1.5 vs 60.0 min) when compared to the conventional CGE method in denaturing conditions.

Examining the postpeak region under denaturing conditions risks omitting valuable information regarding covalent vs noncovalent aggregates. To characterize mRNA in its native form, SEC stands as a fundamental technique for its proficiency in exploring the structural characteristics, purity, and aggregation states of mRNA.[30,31]

To gather information on covalent and noncovalent aggregates, samples were analyzed by SEC, under native and denaturing conditions. Under native conditions, both mCE

https://doi.org/10.1021/acs.analchem.3c05539
Anal. Chem. 2024, 96, 3886−3897

Table 1. Determination of the Nucleotide Number and Abundance Values of Different Size Variants of Several mRNA Samples Obtained by MP[a]

	expected—nucleotide number (nt)/MWs (kDa)	calculated—average nucleotide number (nt)		RSD (%)		difference (%)		abundance (%)	
		monomer	dimer/trimer	monomer	dimer/trimer	monomer	dimer/trimer	monomer	dimer/trimer
mRNA−	683/220.78	668	1356	1.8	2.1	2.2	0.7	83	2
mRNA+	783/254.05	771	1556	2.0	1.2	1.9	1.1	65	16
eGFP mRNA A	980/319.79	979	1991/2958	1.9	0.7/1.2	1.3	1.6/0.9	60	15/5
Fluc mRNA A	1909/622.23	1927	3893	2.9	2.6	2.1	2.0	47	7
beta gal mRNA B	3420/—	3478	6822	0.8	2.1	1.7	0.3	58	2

[a]Data were obtained from three measurements performed on different days for each mRNA sample.

and SEC consistently indicated the presence of aggregates for two mRNA samples (Figure 3c,e), highlighting the potential difficulties in achieving high purity. Interestingly, mCE offers a better separation compared to the SEC. For example, a baseline separation was observed between the monomer and aggregates for eGFP A mRNA, with a distinct separation of two forms of aggregates in mCE (Figure 3c, top trace). The results confirmed an improved separation for the aggregates with the mCE. The percentages of the prepeak/main peaks and aggregates obtained for the two methods are reported in Figure 3d,e (represented with striped bars), showing similar values between the SEC and mCE.

According to published reports,[20,32] the level of mRNA aggregates can be significantly reduced after a heating step (70 °C for 10 min, denaturing condition). Similar results were obtained with both methods (Figure 3c,e, represented with solid bars). For example, a decrease from 47.3 to 8.9% and from 41.0 to 3.5% was observed for the content of aggregates of eGFP A when using mCE and SEC, respectively (Figure 3d,f). This reduction involves the presence of noncovalent aggregates, as they were susceptible to thermal disruption. However, a small fraction of the aggregates exhibited resistance to heating, suggesting their covalent nature.[33,34]

Overall, it is noteworthy that mCE provided the same informative results as conventional CGE and SEC but with a notably smaller amount of material and in a significantly shorter time (<1.5 min). This underlines the advantages of mCE as an efficient and resource-saving alternative for assessing the purity and aggregated content of mRNAs. Having demonstrated the diversity of mRNA aggregates, further investigations are needed to fully characterize them.

Observation of dsRNA 3′-Loop Back Byproducts in CGE and IP-RPLC Profiles. Recent studies have identified two main types of dsRNA byproducts in the IVT reaction.[33] The first is formed by the 3′-loop back of the runoff products to extend the transcription using the opposite strand of DNA as the template, resulting in RNA duplexes (i.e., covalent structures). The second type of dsRNA molecules is formed by the hybridization of antisense RNA molecules to the runoff transcript (i.e., noncovalent structures).[35] These dsRNA byproducts can affect the potency and safety of the mRNA, particularly in therapeutic applications,[36] necessitating additional purification steps to remove dsRNA from the final mRNA product. Two strategies are commonly used to reduce the dsRNA burden. One is the purification of mRNA products using chromatography;[37] the other is the modification of the IVT conditions to decrease byproduct formation. Recently, different engineered T7 polymerases with mutation-enhancing termination efficiency at the intended termination site have been designed to reduce the likelihood of read-through transcription and minimize or prevent the synthesis of these byproducts.[35,38]

Based on our previous results, which showed a reduction in aggregates under denaturing conditions (see Figure 3)—mainly noncovalent forms (potentially antisense transcripts), we were interested in the remaining covalent forms, persisting under the denaturing conditions used in IP-RPLC and CGE.

Several in-house eGFP mRNA constructs were produced using three different polymerases, called wild-type T7 (WT), T7-1, and T7-2. Working under denaturing conditions has proven effective in reducing various noncovalent dsRNAs, although it does not significantly impact dsRNA 3′-loop back byproducts. Analyzing this phenomenon through IP-RPLC and mCE techniques, we first noticed a more pronounced postpeak in IP-RPLC (average of dsRNA percent among mRNA with different T7 polymerases: 9.5% ± 8.0 and 17.6% ± 8.9 for mCE and IP-RPLC, respectively), remaining consistent with its milder denaturing conditions (Figure 4a,b). However, in both methods, the adoption of alternative polymerases compared to WT T7 resulted in a notable reduction of dsRNA 3′-loop back byproducts, confirming the association between the postpeak and these undesired byproducts. Indeed, for mCE, we observed 6.5% (T7-1) and 3.4% (T7-2) of dsRNA when using alternative T7 polymerase compared to 18.6% for the WT T7, while we observed 13.7 and 11.3% versus 27.8% with IP-RPLC.

To confirm these observations, a dot blot—another tool used to detect long dsRNA byproducts—was employed (Figure 4d). This is an immunoblot-based assay that depends on the recognition of the dsRNA byproducts in the reaction with a dsRNA-specific antibody, thus allowing for its semiquantitative analysis. Notably, the T7 polymerase WT exhibited a prominent signal in the dot blot assay, indicative of the presence of dsRNA, while the alternative T7 polymerase variants demonstrated weaker signals, suggesting a reduction in dsRNA synthesis.

Extended Characterization of IVT mRNA Using Advanced Analytical Tools. *MP for Determination of Length and Purity Assessment of mRNA.* MP is a novel technology that enables accurate mass measurement of label-free single biomolecules in their native state.[39] Applied to mRNA analysis, MP offers good repeatability in terms of the calculated average nucleotide number for all analyzed samples, with RSD values below 3.0% (see Table 1). The lengths of mRNA− and mRNA+ were determined to be 668 and 771 nts, respectively, with error values below 2.3% for monomers and

https://doi.org/10.1021/acs.analchem.3c05539
Anal. Chem. 2024, 96, 3886−3897

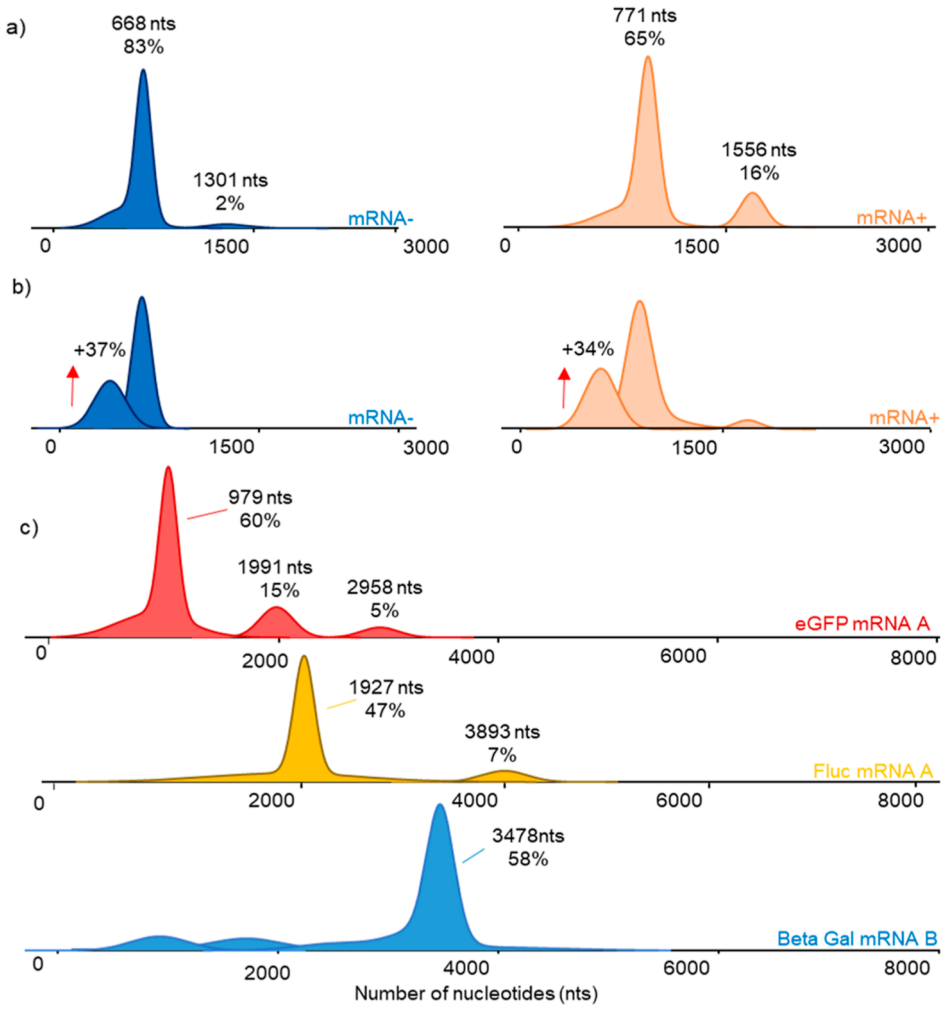

Figure 5. MP measurement of different mRNAs. Profiles were obtained for mRNA− and mRNA+, including (a) control and (b) stress (37 °C, 5 days) samples. (c) Overlay of MP measurements of different mRNAs (eGFP A, Fluc A, and beta gal B) from vendors A and B. The number of nucleotides and relative percentages of size variants of each mRNA are indicated. Arrows indicate the increases in the prepeak region for stressed samples.

2.1% for dimers. As expected, a length difference of ∼100 nts corresponding to the poly(A) tail was observed. Purity levels are aligned with data obtained by IP-RPLC and CGE (Table S2), with values close to 83 and 65% for mRNA− and mRNA+ (see Figure 5a). Interestingly, MP analysis revealed the presence of mRNA dimers for both samples but with a higher level for mRNA+ (∼17%). Dimers were considered non-covalent forms on the basis of their absence in the IP-RPLC and CGE profiles.

Stressed mRNA samples were then analyzed (Figure 5b). The disruption of mRNA dimers was observed, probably caused by heat-stress conditions. Prepeaks for mRNA and mRNA+ increased by 37 and 34%, respectively, compared to control samples, in agreement with data previously obtained by CGE (see Table S2), showing that MP is also a stability-indicating method for mRNAs. It should be noted that high heterogeneity in the prepeak region limited accurate length measurement, illustrating the instrument's current limitations for complex samples.

The applicability of this technology for larger mRNAs, up to 3500 nts were then tested. As shown in Figure 5c, these measurements highlight the wide mass range amenable to MP and the high dynamic range afforded by the single-molecule nature of the measurement. Consistent measurements of mRNA lengths were observed with calculated errors of less than 2.3% (see Table 1), demonstrating the robustness and accuracy of MP as a reliable tool for accurately determining mRNA length across a wide range of sizes.

MP technology provides valuable additional information, particularly for the detection of noncovalent species. For example, the two aggregate forms previously observed in the mCE electropherogram for eGFP A mRNA (Figure 3c, top trace) were successfully identified as a dimer and a trimer, with lengths of 1991 and 2958 nts, respectively (see Table 1 and Figure 5c). Furthermore, this technology may hold promise for determining the average number of nucleotides and percentage purity of each mRNA in complex mixtures, under size difference conditions of >300 nts. Compared to the SEC−multi-angle light scattering (MALS) technique for measuring aggregates, MP does not require a large amount of mRNA sample (only 50 ng versus a few μgs) and does not suffer from poor separation resolution due to the limited pore size of SEC columns, enabling efficient separation of different aggregate forms (see Figure 5c). Overall, the data confirm the great potential of MP technology to be integrated into our analytical

https://doi.org/10.1021/acs.analchem.3c05539
Anal. Chem. 2024, 96, 3886−3897

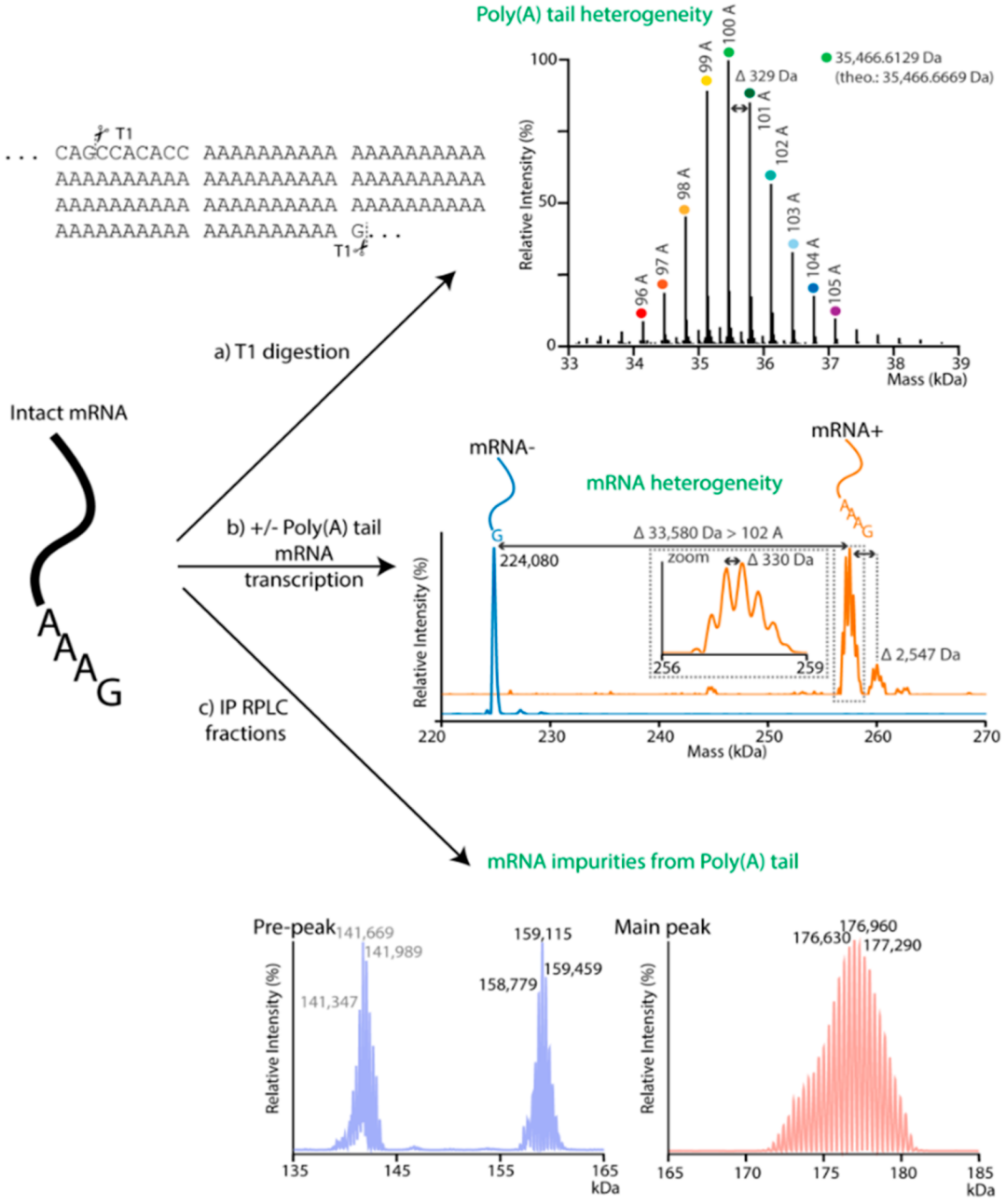

Figure 6. Characterization of mRNA variants by native MS. (a) Poly(A) tail analysis upon T1 cleavage of intact mRNA. T1 cleavage sites of the applied poly(A) sequence are displayed as well as the deconvoluted mass spectrum. The increment of an adenosine residue (+329 Da) is represented by different colored dots. (b) Superposition of the deconvoluted spectra of mRNA+ and mRNA−, showing a mass difference of 33,580 Da corresponding to >102 adenosine residues. (c) Deconvoluted spectra obtained for prepeak (left) and main peak (right) fractions after fractionation from IP-RPLC separation of an in-house mRNA construct (∼580 nts). All MS raw spectra are displayed in Figure S7. Three different mRNAs (mRNA−, mRNA+, and 580 nt mRNA) were analyzed.

toolbox as a fast and simple orthogonal method that provides insights into the homogeneity and stability of mRNA samples.

Native MS for Analysis of the Poly(A) Tail, Intact mRNA, and mRNA Impurities. MS is a key technology for the structural characterization of oligonucleotides[40] and IVT mRNA.[23,24] Although some recent reports have succeeded in sequencing mRNA digests by LC-MS,[28] the analysis of intact RNA is still limited to relatively short oligonucleotides (up to 100 nt). Denaturing conditions and negative ionization mode are commonly applied due to the mobile phase compositions in IP-RPLC−MS approaches. Positive ionization of intact oligonucleotides has been recently demonstrated (25 nts, intact mass <10 kDa) but showed low spectra quality even for short sequences. Generally, the adduct formation propensities of mRNA and inherent mRNA heterogeneity are the major challenges for intact analysis.[41] The major heterogeneity of the mRNA mass profiles is mostly related to the poly(A) tail. We demonstrated the intact mass analysis of mRNA at different analysis levels, focusing on the poly(A) tail heterogeneity, intact mRNA with and without poly(A) tail, and mRNA impurity fractions obtained from IP-RPLC (Figure 6).

Intact MS analysis of the poly(A) tail (around 100 nt) upon T1 cleavage was achieved at isotopic resolution and showed a distribution from 95 to 110 adenosine residues with a high

https://doi.org/10.1021/acs.analchem.3c05539
Anal. Chem. 2024, 96, 3886−3897

mass accuracy of below 2 ppm for major variants (Figure 6). Targeted analysis of the poly(A) tail provides a smaller mass and reduced heterogeneity, allowing a detailed assessment of the poly(A) tail heterogeneity, which is of high relevance for structural characterization of mRNA. It also facilitates the interpretation of intact mRNA analysis. An mRNA transcribed without the poly(A) tail (mRNA−, 683 nt) showed only one average mass at 224.080 kDa under the applied resolution, which is in line with the high-purity of mRNA− determined by IP-RPLC and CGE (see Figure 2). In contrast, the intact mass profile of mRNA+ (783 nt) showed a higher heterogeneity with partial resolution of adenosines (Δ 329 Da) and the expected mass difference to mRNA−, corresponding to the additional poly(A) tail. It should be noted that the experimental mass of both mRNA− and mRNA+ was approximately 3−4 kDa higher than the expected mass (Table 1), which was attributed to the presence of non-covalently bound nucleotide fragments, such as aborted transcripts, which are expected to be retained under the measurement conditions.[33] Furthermore, intact mass analysis of mRNA+ resolved additional minor variants, with a mass difference of 2.5 kDa corresponding to a small number of extra nucleotides in addition to the overall length (i.e., <10 nts). These additional variants were not detected for the mRNA−, suggesting that these variants can correspond to small dsRNA 3′-loop back byproducts.

Finally, intact mass analysis was applied to further characterize mRNA impurities obtained after fractionation from IP-RPLC (Figure S5). We selected a short in-house-produced mRNA construct of around 580 nts, including a 100 nt poly(A) tail, in order to sufficiently resolve minor variants under the applied conditions. An average intact mass of 176.960 kDa was obtained for the main peak (Figure 6). As expected, the main heterogeneity was assigned to the distribution of the poly(A) tail, as confirmed by the mass differences between peaks (±0.3 kDa). A broad distribution of the poly(A) tail, approximately 100 nucleotides in length, with a range of plus or minus 15 nucleotides, was assigned for the fractionated main peak. In contrast, the prepeak fraction showed two main clusters of peaks comprising masses of around 141 and 159 kDa, suggesting the presence of two mRNA impurities. For the 159 kDa mRNA variant, it is interesting to note a less pronounced tail distribution compared to the intact mRNA (right panel, Figure 6c), suggesting a smaller poly(A) tail size. This can be attributed to either abortive addition or partial hydrolysis of the poly(A) tail. Furthermore, subtracting the mass of the main peak by the 141 kDa mRNA variant gives a value of 35 kDa, corresponding to the size of a poly(A) tail of 100 nucleotides, as observed previously (Figure 6b). The intact mass data of the prepeak suggest that these two impurities correspond to the full length of the mRNA with partial or complete absence of the poly(A) tail chain.

Further investigations were performed to confirm that impurities in the prepeak fraction do not arise from other deletions within the mRNA structure. For this, we used Oxford Nanopore direct RNA sequencing as an orthogonal method (Experimental Section S4). In line with the observed differences in MS, the prepeak fraction showed a slightly higher proportion of short reads (i.e., the number of base pairs sequenced), suggesting potential differences in the molecular composition of this fraction compared with the main peak fraction (see Figure S6). Furthermore, full mRNA coverage and absence of deletions were confirmed for the 5′- and 3′-UTRs and the ORF for both fractions (prepeak and main peak). Consequently, the impurities present in the prepeak region were attributed to mRNA variants with different poly(A) tail lengths.

In summary, we successfully demonstrated that native MS in positive mode without separation enables us to characterize poly(A) tails around 100 nts in length with high accuracy at isotopic resolution and mRNA at the intact level (up to 750 nts), which has not been demonstrated previously. Intact mass analysis provided more detailed molecular information on mRNA integrity and heterogeneity, making it an excellent tool for the extensive characterization of mRNA impurities. The analytical advantages of MS underscore the integrity and characteristics of therapeutic mRNA, providing valuable insights into the development and quality assessment of mRNA-based treatments and thereby contributing significantly to the pharmaceutical field.

CONCLUSIONS

In this study, we reported a diverse range of analytical technologies, incorporating both established and novel analytical methods, to offer comprehensive profiling of mRNA impurities. Both IP-RPLC and CGE techniques are effective in assessing the purity of mRNA species, revealing strong similarities in their separation patterns. These methods indicated the presence of an mRNA variant without a poly(A) tail and can discriminate species containing a partial poly(A) tail in the prepeak region. However, the distinction becomes clear for impurities present in the postpeak region, where CGE exhibits higher resolution due to its stronger denaturation conditions than IP-RPLC, for more accurate quantification. We also underlined the potential of mCE, which enabled us to confirm the results obtained with CGE and SEC, while requiring substantially fewer sample and turnaround time. In the comparative study with SEC, mCE proved to be a more promising choice for measuring aggregate content with better separation of the different forms. Although further work is required to implement the mCE technology in a GMP environment (i.e., robustness, reliability, accuracy, etc.), this tool should be part of the analytical toolbox for development work. The subsequent application of MP highlighted the results obtained using mCE and had a great advantage of providing a highly accurate measurement of the length of mRNAs, including their various aggregate forms (i.e., dimers and trimers). Finally, native MS played a crucial role in monitoring impurities in the postpeak region with accuracy at sufficient resolution to reflect the different lengths of the poly(A) tail. This holistic study demonstrates the capacity of these analytical methods to characterize mRNA and its related impurities.

Our work pinpointed prepeak impurities as mRNA variants with different poly(A) tail lengths due to aborted additions or partial hydrolysis, potentially compromising mRNA stability, a critical attribute in mRNA-based therapeutics and vaccines, underlining the paramount need for poly(A) tail control. On the other hand, postpeak impurities were linked to various dsRNA conformations, known for their immunogenic activity, underscoring the need to monitor their level. Collectively, our study underscores the utmost importance of developing robust technologies for assessing mRNA purity and characterizing impurities, particularly their biological effects. Ultimately, this work represents a pivotal statement in advancing the QC and

https://doi.org/10.1021/acs.analchem.3c05539
Anal. Chem. 2024, 96, 3886−3897

assessment of mRNA products, with far-reaching implications for pharmaceutical science and patient care.

■ ASSOCIATED CONTENT

Supporting Information

The Supporting Information is available free of charge at https://pubs.acs.org/doi/10.1021/acs.analchem.3c05539.

IVT reaction and capping protocol for in-house mRNAs, poly(A) tail cleavage and purification procedures, dot blot protocol for dsRNA analysis, Oxford Nanopore direct RNA: library preparation, sequencing, and analysis, effect of capillary temperature on eGFP mRNA analysis by CGE−LIF, IP-RPLC−UV and CGE−LIF profiles for mRNA samples, poly(A) tail analysis of eGFP mRNAs obtained from different suppliers by IP-RPLC−UV, correlation between poly(A) tail length and the level of prepeak regions, chromatograms of prepeak and main peak fractions obtained after fractionation from IP-RPLC of an in-house mRNA construct, NGS sequencing data obtained for eGFP mRNA, raw data from native MS analysis for intact mRNA characterization, as well as poly(A) tail length and distribution, purity values of different eGFP mRNAs obtained by IP-RPLC and CGE−LIF, and purity values of different mRNA− and mRNA+ samples, including a control and a stress condition for each, obtained by IP-RPLC and CGE (PDF)

■ AUTHOR INFORMATION

Corresponding Authors

Julien Camperi − *Cell Therapy Engineering and Development, Genentech, South San Francisco, California 94080, United States;* orcid.org/0000-0002-4020-2278; Email: camperij@gene.com

Axel Guilbaud − *Protein Analytical Chemistry, Genentech, South San Francisco, California 94080, United States;* Email: guilbaua@gene.com

Authors

Steffen Lippold − *Protein Analytical Chemistry, Genentech, South San Francisco, California 94080, United States;* orcid.org/0000-0002-1032-5808

Luladey Ayalew − *Cell Therapy Engineering and Development, Genentech, South San Francisco, California 94080, United States*

Brian Roper − *Cell Therapy Engineering and Development, Genentech, South San Francisco, California 94080, United States*

Stephanie Shao − *Cell Therapy Engineering and Development, Genentech, South San Francisco, California 94080, United States*

Emily Freund − *Department of Molecular Biology, Genentech, South San Francisco, California 94080, United States*

Ariane Nissenbaum − *Department of Molecular Biology, Genentech, South San Francisco, California 94080, United States*

Carolina Galan − *Department of Molecular Biology, Genentech, South San Francisco, California 94080, United States*

Qinjingwen Cao − *Protein Analytical Chemistry, Genentech, South San Francisco, California 94080, United States*

Feng Yang − *Protein Analytical Chemistry, Genentech, South San Francisco, California 94080, United States;* orcid.org/0000-0003-0769-5573

Christopher Yu − *Cell Therapy Engineering and Development, Genentech, South San Francisco, California 94080, United States*

Complete contact information is available at: https://pubs.acs.org/10.1021/acs.analchem.3c05539

Notes

The authors declare no competing financial interest.

■ ACKNOWLEDGMENTS

The authors acknowledge Dayue Chen from Genentech (South San Francisco, CA) for a critical review of this article. The authors also thank Brenda Watt from Refeyn (Portland, OR) for valuable advice on mass photometry.

■ REFERENCES

(1) Pardi, N.; Hogan, M. J.; Porter, F. W.; Weissman, D. *Nat. Rev. Drug Discovery* **2018**, *17* (4), 261−279.

(2) Rhoads, R. E. Synthetic mRNA: Production, Introduction into Cells, and Physiological Consequences. In *Synthetic mRNA*; Rhoads, R. E., Ed.; *Methods in Molecular Biology*; Springer New York: New York, NY, 2016; Vol. *1428*, pp 3−27.

(3) Miao, L.; Zhang, Y.; Huang, L. *Mol. Cancer* **2021**, *20* (1), 41.

(4) Beck, J. D.; Reidenbach, D.; Salomon, N.; Sahin, U.; Türeci, Ö.; Vormehr, M.; Kranz, L. M. *Mol. Cancer* **2021**, *20* (1), 69.

(5) Sahin, U.; Karikó, K.; Türeci, Ö. *Nat. Rev. Drug Discovery* **2014**, *13* (10), 759−780.

(6) Kwon, S.; Kwon, M.; Im, S.; Lee, K.; Lee, H. *Arch. Pharm. Res.* **2022**, *45* (4), 245−262.

(7) Domazet-Lošo, T. *Genes* **2022**, *13* (5), 719.

(8) Guimaraes, G. J.; Kim, J.; Bartlett, M. G. *Mass Spectrom. Rev.* **2023**, 21856.

(9) Demelenne, A.; Servais, A.-C.; Crommen, J.; Fillet, M. *J. Chromatogr. A* **2021**, *1651*, 462283.

(10) Goyon, A.; Fan, Y.; Zhang, K. Analysis of Oligonucleotides by Liquid Chromatography. *Liquid Chromatography*; Elsevier, 2023; pp 357−380.

(11) Wei, B.; Wang, J.; Cadang, L.; Goyon, A.; Chen, B.; Yang, F.; Zhang, K. *J. Chromatogr. A* **2022**, *1665*, 462839.

(12) Azarani, A. *Nucleic Acids Res.* **2001**, *29* (2), No. e7.

(13) Basiri, B.; Bartlett, M. G. *Bioanalysis* **2014**, *6* (11), 1525−1542.

(14) Currie, J.; Dahlberg; Jacob, R.; Eriksson, J.; Schweikart, F.; Nilsson; Gunilla, A.; Örnskov, E. Stability Indicating Ion-Pair Reversed-phase Liquid Chromatography Method for Modified mRNA, **2021**, preprint; Chemistry.

(15) Lu, T.; Klein, L. J.; Ha, S.; Rustandi, R. R. *J. Chromatogr. A* **2020**, *1618*, 460875.

(16) Skeidsvoll, J.; Ueland, P. M. *Electrophoresis* **1996**, *17* (9), 1512−1517.

(17) Raffaele, J.; Loughney, J. W.; Rustandi, R. R. *Electrophoresis* **2022**, *43* (9−10), 1101−1106.

(18) Donegan, M.; Nguyen, J. M.; Gilar, M. *J. Chromatogr. A* **2022**, *1666*, 462860.

(19) Kuwayama, T.; Ozaki, M.; Shimotsuma, M.; Hirose, T. *Anal. Sci.* **2023**, *39* (3), 417−425.

(20) Goyon, A.; Tang, S.; Fekete, S.; Nguyen, D.; Hofmann, K.; Wang, S.; Shatz-Binder, W.; Fernandez, K. I.; Hecht, E. S.; Lauber, M.; Zhang, K. *Anal. Chem.* **2023**, *95* (40), 15017−15024.

(21) Young, G.; Hundt, N.; Cole, D.; Fineberg, A.; Andrecka, J.; Tyler, A.; Olerinyova, A.; Ansari, A.; Marklund, E. G.; Collier, M. P.; Chandler, S. A.; Tkachenko, O.; Allen, J.; Crispin, M.; Billington, N.; Takagi, Y.; Sellers, J. R.; Eichmann, C.; Selenko, P.; Frey, L.; Riek, R.; Galpin, M. R.; Struwe, W. B.; Benesch, J. L. P.; Kukura, P. *Science* **2018**, *360* (6387), 423−427.

(22) Wagner, C.; Fuchsberger, F. F.; Innthaler, B.; Lemmerer, M.; Birner-Gruenberger, R. *Int. J. Mol. Sci.* **2023**, *24* (13), 11033.
(23) Beverly, M.; Hagen, C.; Slack, O. *Anal. Bioanal. Chem.* **2018**, *410* (6), 1667−1677.
(24) Brouze, A.; Krawczyk, P. S.; Dziembowski, A.; Mroczek, S. *WIREs RNA* **2023**, *14* (1), No. e1737.
(25) Beverly, M.; Dell, A.; Parmar, P.; Houghton, L. *Anal. Bioanal. Chem.* **2016**, *408* (18), 5021−5030.
(26) Lippens, J. L.; Timmons, H. C.; Welch, C.; Kulkarni, A.; Flick, T. G. *J. Am. Soc. Mass Spectrom.* **2023**, *34* (11), 2491−2497.
(27) Brophy, P.; Shion, H.; Doneanu, C.; H Yang, B. D.; Botamanenko, D.; Abbatiello, S.; Jarrell, A.; Koza, S.; Yu, Y.; Giles, K.; Jarrold, M. Characterization of Intact mRNA Using IP-RP-TOF-MS, SEC MALS and CDMS. Poster. 2023, https://www.waters.com/webassets/cms/library/docs/2022asms_doneanu_cdms.pdf.
(28) Gau, B. C.; Dawdy, A. W.; Wang, H. L.; Bare, B.; Castaneda, C. H.; Friese, O. V.; Thompson, M. S.; Lerch, T. F.; Cirelli, D. J.; Rouse, J. C. *Sci. Rep.* **2023**, *13* (1), 9038.
(29) Patel, H. K.; Zhang, K.; Utegg, R.; Stephens, E.; Salem, S.; Welch, H.; Grobe, S.; Schlereth, J.; Kuhn, A. N.; Ryczek, J.; Cirelli, D. J.; Lerch, T. F. *J. Pharm. Sci.* **2023**, *112* (5), 1364−1371.
(30) Feng, X.; Su, Z.; Cheng, Y.; Ma, G.; Zhang, S. *J. Chromatogr. A* **2023**, *1707*, 464321.
(31) Kloczewiak, M.; Banks, J. M.; Jin, L.; Brader, M. L. *Mol. Pharmaceutics* **2022**, *19* (7), 2022−2031.
(32) Camperi, J.; Moshref, M.; Dai, L.; Lee, H. Y. *Anal. Chem.* **2021**, *94*, 1432−1440.
(33) Nwokeoji, A. O.; Kumar, S.; Kilby, P. M.; Portwood, D. E.; Hobbs, J. K.; Dickman, M. J. *Analyst* **2019**, *144* (16), 4985−4994.
(34) Roy, B. Understanding and Overcoming the Immune Response from Synthetic mRNAs. 2019, https://www.genengnews.com/resources/understanding-and-overcoming-the-immune-response-from-synthetic-mrnas-2/.
(35) Dousis, A.; Ravichandran, K.; Hobert, E. M.; Moore, M. J.; Rabideau, A. E. *Nat. Biotechnol.* **2023**, *41* (4), 560−568.
(36) Karikó, K.; Muramatsu, H.; Ludwig, J.; Weissman, D. *Nucleic Acids Res.* **2011**, *39* (21), No. e142.
(37) Baiersdörfer, M.; Boros, G.; Muramatsu, H.; Mahiny, A.; Vlatkovic, I.; Sahin, U.; Karikó, K. *Mol. Ther.–Nucleic Acids* **2019**, *15*, 26−35.
(38) Miller, M.; Alvizo, O.; Chng, C.; Jenne, S.; Mayo, M.; Mukherjee, A.; Sundseth, S.; Chintala, A.; Penfield, J.; Riggins, J.; Zhang, X.; Sero, A.; Dassie, J.; Leatherbury, N.; Baskerville, S.; Huisman, G. An Engineered T7 RNA Polymerase for Efficient Co-transcriptional Capping with Reduced dsRNA Byproducts in mRNA Synthesis, **2022**, preprint; Molecular Biology.
(39) Li, Y.; Struwe, W. B.; Kukura, P. *Nucleic Acids Res.* **2020**, *48* (17), No. e97.
(40) Sutton, J. M.; Guimaraes, G. J.; Annavarapu, V.; Van Dongen, W. D.; Bartlett, M. G. *J. Am. Soc. Mass Spectrom.* **2020**, *31* (9), 1775−1782.
(41) Strezsak, S. R.; Pimentel, A. J.; Hill, I. T.; Beuning, P. J.; Skizim, N. J. *ACS Omega* **2022**, *7* (26), 22181−22191.

https://doi.org/10.1021/acs.analchem.3c05539
Anal. Chem. 2024, 96, 3886−3897